atmosphere

MDPI

Supplementary Materials:

Francesca Costabile [1,*], Stefano Decesari [2], Roberta Vecchi [3], Franco Lucarelli [4,5], Gabriele Curci [6,7], Dario Massabò [8], Matteo Rinaldi [2], Maurizio Gualtieri [9,†], Emanuela Corsini [10], Elena Menegola [11], Silvia Canepari [12], Lorenzo Massimi [12], Stefania Argentini [1], Maurizio Busetto [2], Gianluca Di Iulio [1], Luca Di Liberto [1], Marco Paglione [2], Igor Petenko [1], Mara Russo [2], Angela Marinoni [2], Gianpietro Casasanta [1], Sara Valentini [3], Vera Bernardoni [3], Federica Crova [3], Gianluigi Valli [3], Alice Corina Forello [4], Fabio Giardi [4], Silvia Nava [4,5], Giulia Pazzi [4], Paolo Prati [8], Virginia Vernocchi [8], Teresa La Torretta [9], Ettore Petralia [9], Milena Stracquadanio [9], Gabriele Zanini [9], Gloria Melzi [10], Emma Nozza [3,10], Martina Iulini [10], Donatella Caruso [10], Lucia Cioffi [10], Gabriele Imperato [10], Flavio Giavarini [10], Maria Battistoni [3,11], Francesca Di Renzo [11], Maria Agostina Frezzini [12], Cinzia Perrino [13] and Maria Cristina Facchini [2]

1. PM1 mass and chemical composition - Daily samples characterization

Extractions were performed on sample punches of 1.5 cm2 by 30-min sonication using 5 mL of MilliQ water. Anions analysis was carried out using a solution of Na2CO3 and NaHCO2 as eluent, while cations analysis used MSA (methane-sulfonic acid) as eluent. During Levoglucosan analysis, NaOH was used as eluent. The instrument was periodically calibrated with standard solutions.

2. Ion chromatography

Ionic component and Levoglucosan content were determined via Ion Chromatography (ThermoFisher) analysis on daily quartz-fibre filters. Method detection limits are reported in Table S1.

3. Oxidative and reducing potential

OP^{DTT} was measured by using three aliquots of 0.7 mL for each sample solution incubated at 37 °C with 0.1 mL of DTT (1 mM) and 0.2 mL of potassium phosphate buffer (1 M). Then, 1 mL of trichloroacetic acid (10%TCA) was added to the mixture at different reaction times (0, 10 and 20 minutes) to stop DTT reaction. An aliquot of the reaction mixture (1 mL) was mixed with 2 mL of tris-buffer (0.08 M, containing EDTA 4 mM) and 50 μL of 5,5-dithiobis-2-nitrobenzoic acid (DTNB). The obtained solution was measured at 412 nm by using a UV-Vis spectrometer. OP^{AA} was determined by adding 300 μL of phosphate buffer (0.5 mM) and 100 μL of AA to 2.5 mL of sample solution. Then, the absorbance was measured at 265 nm at different reaction times (0, 10 and 20 minutes) by UV-Vis spectrometry. OP^{DCFH} was measured by dissolving 4.87 mg of 2′,7′-dichlorofluorescin diacetate (DCFH-DA) in 5 mL of ethanol (EtOH, 96%) with 20 mL NaOH (0.01M) and kept in the dark for 30 minutes. Then, 125 μL of DCFH (5 μM) and 5 mL of HRP (0.5 units mL-1) dissolved in a sodium phosphate buffer (pH 7.4; 25 mM) were added to 1.5 mL of the sample solution placed in a water bath at 37 ºC for 5 minutes. The concentration of dichlorofluorescin (DCF) upon reaction with ROS was measured by using fluorescent spectroscopy. RP^{DPPH} was determined using 2 mg of DPPH in 50 mL of ethanol (EtOH 96%). The mixture was shaken for 30 min under magnetic stirrer agitation and kept in the dark. The obtained solution was measured at 517 nm by UV-Vis spectrometry.

For the DTT analysis on quartz fibre filters, 2.5 ml of extract were added to 0.5 ml of potassium phosphate buffer (0.5 M, pH = 7.4) into an amber vial (primary vial). The obtained solution was heated at the temperature of 37°C using a water bath. When the temperature reached the desired value, 30 ml of the DTT solution, with a concentration of 10 mM, were added to the vial at the time zero. At the time of 5, 10, 15, 20 and 25 minutes an aliquot of 0.5 ml was removed from the vial and added to a second amber vial (secondary vial) containing 0.5 ml of 10% trichloroacetic acid to stop the reaction. After all solutions were collected, 50 ml of 10mM DTNB solution in phosphate buffer at pH 7.4 were added

to all secondary vials, mixed adequately, and allowed to react for 5 minutes in the dark. Then, 2 ml of a solution of 0.4 M Tris-HCl buffer at the pH of 8.9 and EDTA 20 mM were added. The reaction between the residual DTT and DTNB forms 2-nitro-5-thiobenzoic acid (TNB), which was quantified at its maximum of absorption at 412 nm wavelength by a TIDAS E (J&M) UV-VIS spectrophotometer.

For both the total and soluble approaches, the kinetics of DTT oxidation was followed by measuring the decrease of the DTT concentration added to the sample (100 μmol) over the reaction course. The DTT depletion rate (nmolDTT min-1), which is proportional to the reactive oxygen species production, was computed as the slope of the straight line obtained by fitting the five experimental points of the DTT concentration as a function of the reaction time (5, 10, 15, 20 and 25 minutes). Slopes obtained by the field blank filters, following the same approach, were subtracted from the slopes of the samples, to compensate for signals coming from the filter matrix. The reproducibility of the method was determined on repeated tests of standard DTT-active organic compounds and resulted the uncertainty on the order of 15% and 30% for the water soluble and total OP, respectively.

4. ChAMBRe instruments and online monitors

The laboratory experiments were conducted in an atmospheric simulation chamber (ASC) and specifically at ChAMBRe (Chamber for Aerosol Modelling and Bio-aerosol Research) [Massabò et al., 2018; Danelli et al., 2021; Vernocchi et al., 2021] in Genoa (www.labfisa.ge.infn.it), which represents a unique facility in Italy. ChAMBRe is a stainless-steel chamber, with a volume of about 2.2 m^3; scattered all over the main body, there are ISO-K flanges, with different diameter, which permit the access to the inner volume. Connected to ChAMBRe, several instruments and online monitors (listed in the Supplementary Material) complete the facility. The whole set-up is managed by a custom NI Labview SCADA (Supervisory Control And Data Acquisition). Inside ChAMBRe, atmospheric conditions (i.e., both chemical and physical parameters) can be maintained and monitored in real time for periods long enough to reproduce realistic environments and to study interactions among their constituents.

During RHAPS, experiments were carried out starting from the exhaust of a soot generator (Mini Inverted Soot Generator - Argonaut Scientific Corp.). Well-characterized particles of BC [Vernocchi et al., 2021], and different mixtures of them with other pollutants, were aged inside ChAMBRe by different mechanisms, such as exposition to oxidant agents (i.e., NO_2 and O_3). Additional seeds (i.e., $(NH_4)_2SO_4$ or NH_4NO_3) were used too. The relative humidity was adjusted at varying levels between experiments. In addition to the online monitors, filter samples were collected for offline analysis of oxidative potential and for in vitro toxicological screening.

Several instruments and online monitors are connected to ChAMBRe (Table S2), and controlled by a remote Ethernet connection and a NI Compact-RIO acquisition module (based on the NI cRIO-9064 controller). In the bottom of the structure, a fan is installed to favour the mixing of gas and aerosol species in the chamber volume. A composite pumping system is connected to ChAMBRe to clean up its volume at the end of each experiment, to avoid possible contamination in the further tests. The system consists of a rotary pump (model TRIVAC® D65B, Leybold Vacuum), followed by a root pump (model RUVAC WAU 251, Leybold Vacuum) and a turbo pump (Leybold Turbovac 1000); it can evacuate the total volume down to 10-5 mbar in about 15 minutes. Between the pumping system and ChAMBRe is collocated a safety valve (Leycon Secuvac DN 63, Oerlikon Leybold Vacuum) as a gate to prevent possible backwashes of the pumps oil inside the chamber. After the evacuation, ChAMBRe is refilled with ambient air filtered by several pollutant traps (including a HEPA filter and zeolite traps).

5. Quantification of polycyclic aromatic hydrocarbons (PAH)

Reagents and chemicals

Benzo(α)anthracene, chrysene, benzo(β)fluoranthene, benzo(α)pyrene and benzo(α)anthracene - D12 were purchased from SUPELCO 959 (North Harrison Road, PA, USA).

Acetonitrile (ACN) and dichloromethane (CH_2Cl_2) were bought from Carlo Erba Reagents s.r.l. (Cornaredo, Italy).

PAHs extraction protocol

The concentration of PAHs, such as benzo(α)anthracene, chrysene, benzo(β)fluoranthene and benzo(α)pyrene were evaluated in quartz filters previously exposed during the winter sampling in two different areas (i.e. Bologna and San Pietro Capofiume, Italy).

The samples were prepared according to [Terzopoulou et al., 2015; Gosetti et al., 2011] with some modifications.

Before the extraction, filters were weighted individually on analytical balance. For the quantitative analysis benz(α)anthracene-D12 was added as internal standard (200ng/sample) to all filters.

Every sample was dissolved in 7,0 mL of CH_2Cl_2 and the suspension was separated from its solid fraction through filter paper. Samples were dried under nitrogen gas flow (N_2) and 5,0 mL of ACN were added. After vortexing, samples were filtered by 0,45 μM regenerated cellulose membrane filters and each solution was concentrated until 1,0 mL under N_2 gas flow. Finally, samples were purified by 0,22μM regenerated cellulose membrane filters and dried under N_2 gas flow. The extracts were reconstituted in 20 μL of ACN before the injection.

Gas-Chromatography Mass Spectrometry (GC-MS)

The quantitative analysis was performed using gas chromatography (Varian 3900 GC) supplied by ion trap mass spectrometry (Varian Saturn 2100T). The chromatographic separation was achieved with TG-5SILMS column. The injector temperature was 280 °C, the flow rate was 1,0 ml/min and the gradient was as follow: 0-2.00 min 80°C, 2.00-22.00 min linear gradient to 300 °C (10 °C/min) and 22.00-38.00 min maintained at 300°C.

As concerned mass spectrometry conditions, electron impact ion source was set at 70 eV and detector ion trap mass range scan was 100-400 milli mass unit (mmu). Quantitative analysis was performed on the basis of calibration curves freshly prepared.

Table S3 shows the m/z ratio and retention time of the analytes and IS.

6. Assessment of the forecasting skills

The main motivation for the implementation of the operational forecast system was to provide information for the scheduling of the SIOPs, which had to be planned at least one week in advance. The main question was to support the field measurement strategy with the identification of source-specific aerosol types for which we aimed at selecting periods having favorable conditions for the accumulation of pollutants, the production of secondary aerosol, minimal interference from dust advected from the Sahara Desert. We thus looked for anticyclonic condition over the Western Mediterranean, low chance of advection from Sahara and low chance of rainy and windy conditions.

In Figure S1 we illustrate the broad forecasting skills of the modelling system. In panel (a) we display the decay of spatial correlation of the sea levels pressure field from GFS forecast as a function of daily lead time. We found a winter campaign-average correlation near 1 for the first three days and above 0.8 until day 7.

Afterwards, we found a sharper and gradual decrease down to 0.35 until day 13, and then a plateau until day 16. To understand the impact of the spatial correlation decay, we display in Figure 7 an example of the sea level pressure field averaged during a potential

SIOP campaign week (from Tuesday to Saturday) obtained from the analysis (D00) and the forecasts 5, 10 and 15 days ahead, alternatively. The difference between the 5-day-ahead forecast the analysis looks very small: both the location and the magnitude of the main synoptic scale features are very similar, with only fine differences in the simulated patterns. At day-10 forecast time, more substantial differences emerge: the low pressure near Iceland is shallower with respect to the analysis, the high pressure over Northern Africa is less prominent, while high pressure over Eastern-Central Europe is more prominent, with the appearance of a secondary high pressure center over Scandinavia. At day-15 forecast time, the Iceland low is retreated northward by an expanded Azores high, and the high pressure over Central Europe is much less marked. However, over the Mediterranean basin general anticyclonic conditions, with air masses slowly advected from the southern quadrants, are deducible at all lead times. This relative stability and reliability at least of the very broad synoptic features over the area of interest (Northern Italy) was a common feature during the campaigns (both in winter and summer, see Figure S 4 for the latter), which made the information derived from the forecast system effectively useful for the SIOP scheduling.

In panels (b-d) of Figure S1 we illustrate model skills from the local perspective. In panel (b) we show the temporal correlation as a function of lead time of the temperature in Bologna between the analysis (day-0) and the forecasts, averaged over the winter campaign period (for summer campaign refer to Figure S 4). We found a correlation of 0.8 until day-2, then a constant correlation around 0.6 until day-11, and a sharp decrease afterwards. For the summer case (Figure S 1 (b)), the correlation decay was more gradual. In panel (c) we compare the observed daily mean temperature timeseries in Bologna, with the timeseries from WRF forecasts at 5, 10, and 15 days lead time. The broad trend is captured at all forecast lead times, in terms of increasing and decreasing periods, but with increasing "noise" with increasing lead time. Remarkably, the drop of temperatures between 10 and 14 of February, and the subsequent reprise, was correctly anticipated at day-5 and day-10, but was less clear at day-15. This confirmed the reliability of forecast information at least of the broad features until at least day-10, which was enough for a correct scheduling of the SIOPs. In panel (d), we compare the observed $PM_{2.5}$ timeseries in Bologna with the timeseries forecasted with CHIMERE. The skill of the model here is more difficult to assess, given the generally larger bias with respect to the meteorological variables. For example, the enhanced concentrations in some subperiods (e.g. 02-06 Jan, 16-26 Feb, 02-05 Mar) were reasonably anticipated at day-5, but with much less reliability at day-10 and day-15. Indeed, the SIOP planning relied more heavily on an evaluation of the synoptic scale meteorological forecasts, rather than a point-wise evaluation of the chemical variables.

SUPPLEMENTARY FIGURES

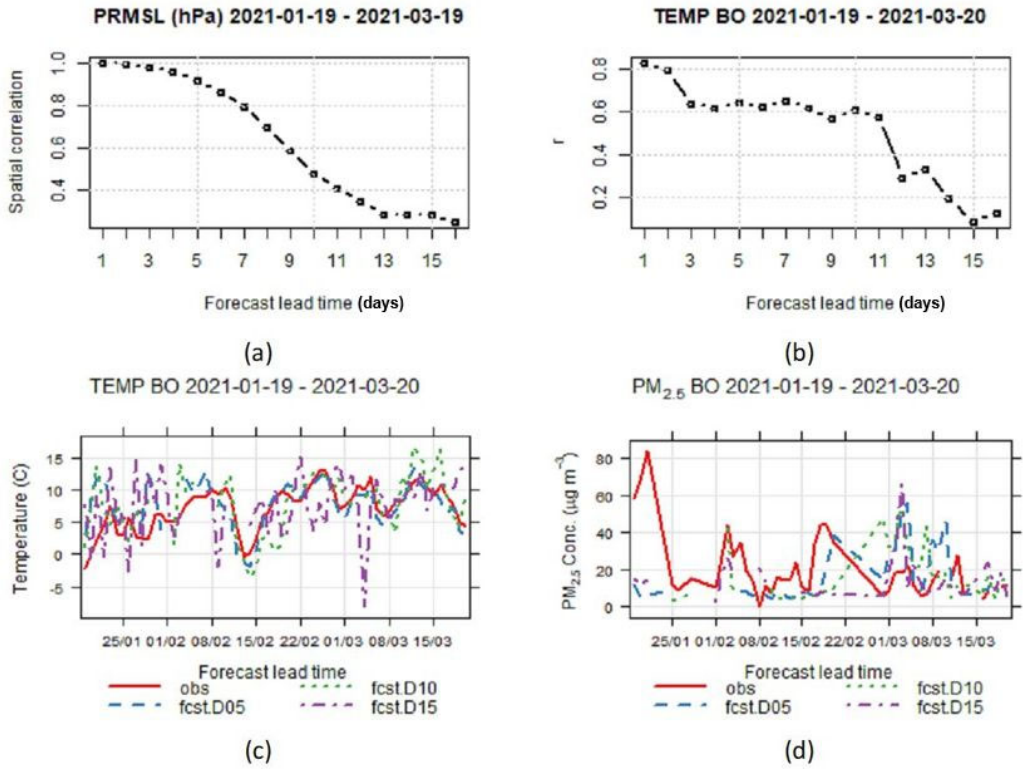

Figure S1. Illustration of forecast system skills during winter campaign. (a) Spatial correlation of sea levels pressure at 00 UTC from NOAA/GFS simulation between analysis and forecast days from 1 to 16. (b) Temporal correlation of daily mean temperature in Bologna from WRF simulation between analysis and forecast days from 1 to 16. (c) Timeseries of daily mean temperature in Bologna during winter campaign from observations and WRF simulation on forecast days 5, 10, and 15. (d) Timeseries of daily mean PM2.5 concentration in Bologna during winter campaign from observations and CHIMERE simulation on forecast days 5, 10, 15.

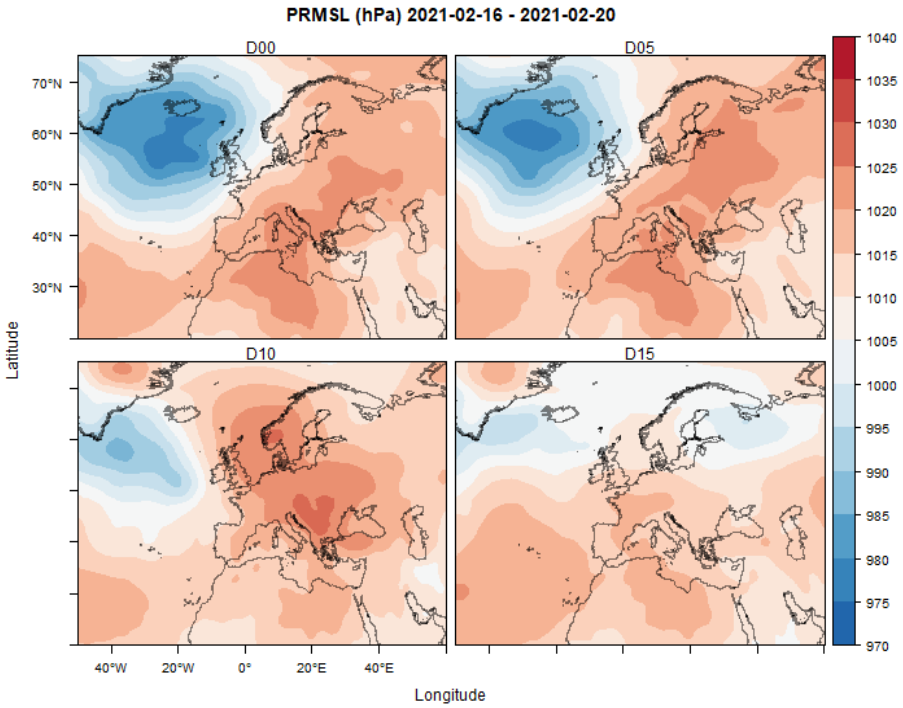

Figure S2. Average sea level pressure at 00 UTC from NOAA/GFS simulation in the period 16-20 Feb 2021 (SIOP3): maps for analysis (D00) and forecast 5, 10 and 15 days ahead (D05, D10, D15).

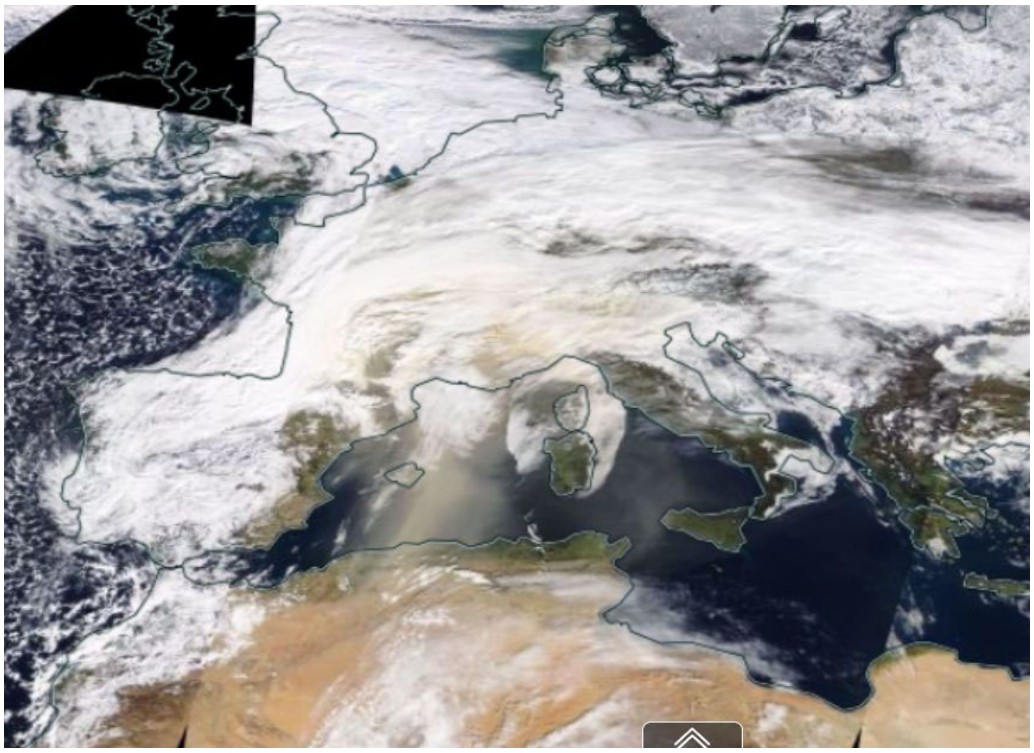

Figure S3. MODIS/Terra true color image over Western Europe on 6 Feb 2021. A Saharan dust plume advected over the low-cloud deck covering Northern Italy is visible. Image from NASA WorldView.

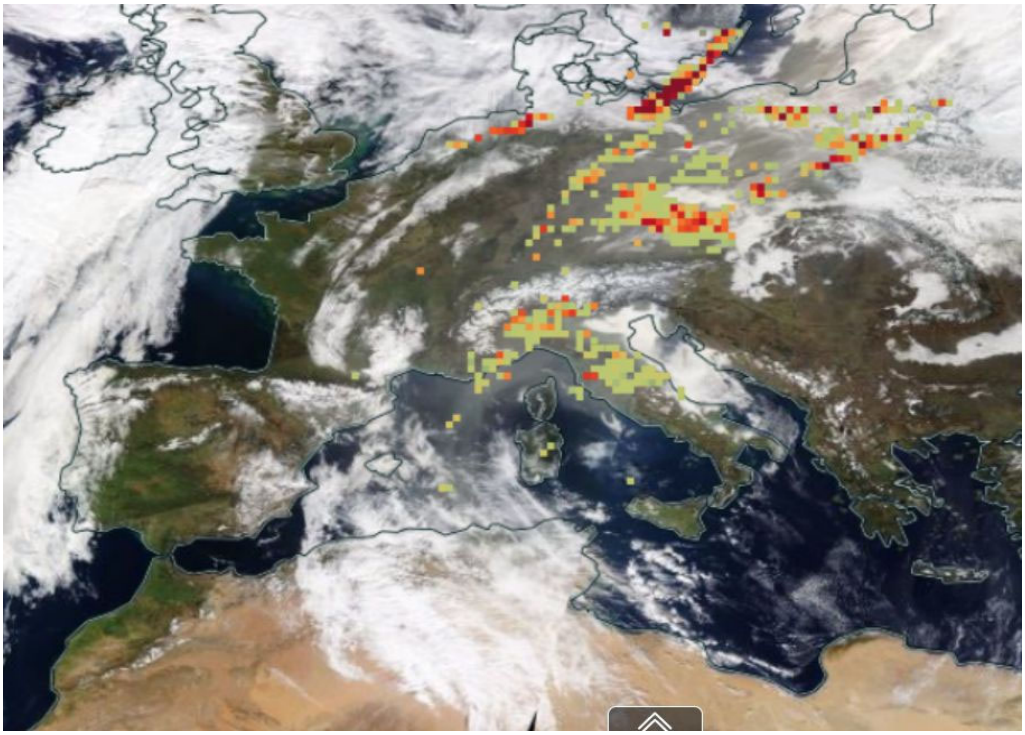

Figure S4. MODIS/Terra true color image over Western Europe on 23 Feb 2021. Superimposed the Dust Index from AIRS/Aqua. A Saharan dust plume advected over Northern Italy is visible. Image from NASA WorldView.

Figure S5. MODIS/Terra true color image over Western Europe on 21 Jun 2021. A dust plume is visible over Italy. Image from NASA WorldView.

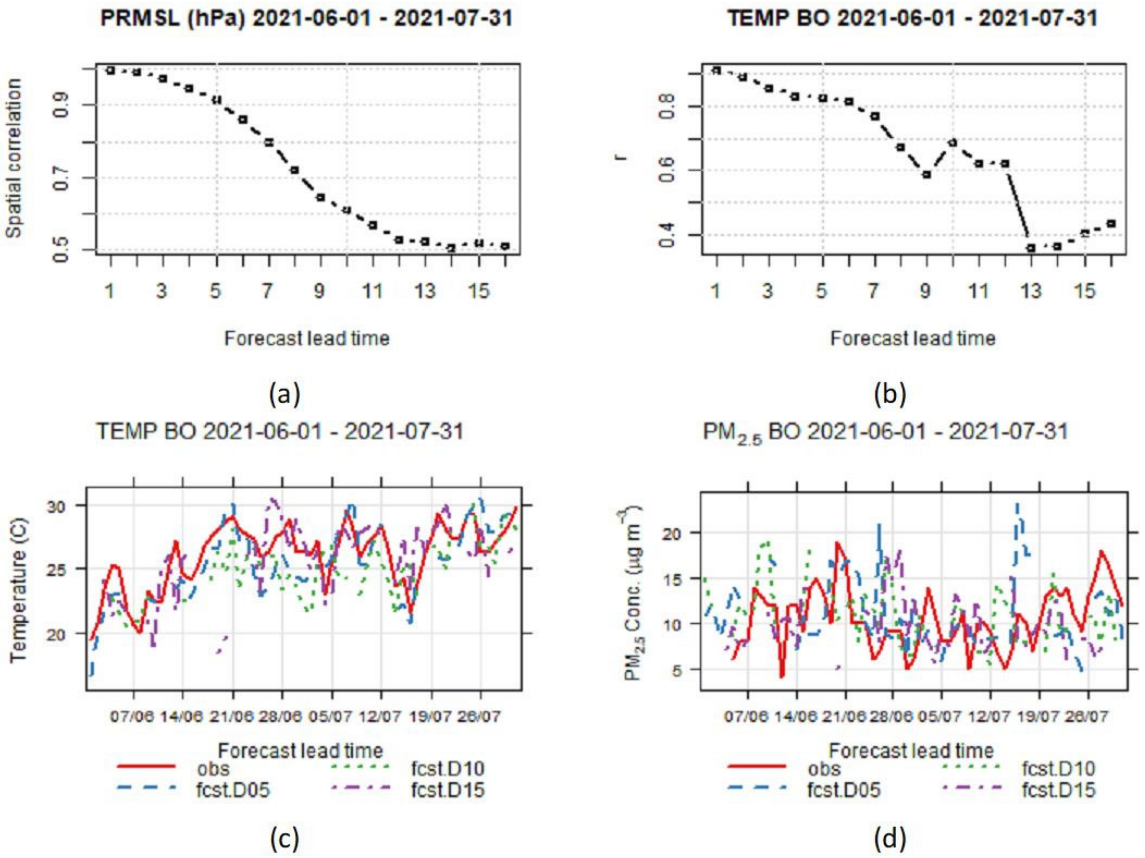

Figure S6. Illustration of forecast system skills during summer campaign. (a) Spatial correlation of sea levels pressure at 00 UTC from NOAA/GFS simulation between analysis and forecast days from 1 to 16. (b) Temporal correlation of daily mean temperature in Bologna from WRF simulation between analysis and forecast days from 1 to 16. (c) Timeseries of daily mean temperature in Bologna during winter campaign from observations and WRF simulation on forecast days 5, 10, and 15. (d) Timeseries of daily mean PM2.5 concentration in Bologna during winter campaign from observations and CHIMERE simulation on forecast days 5, 10, 15.

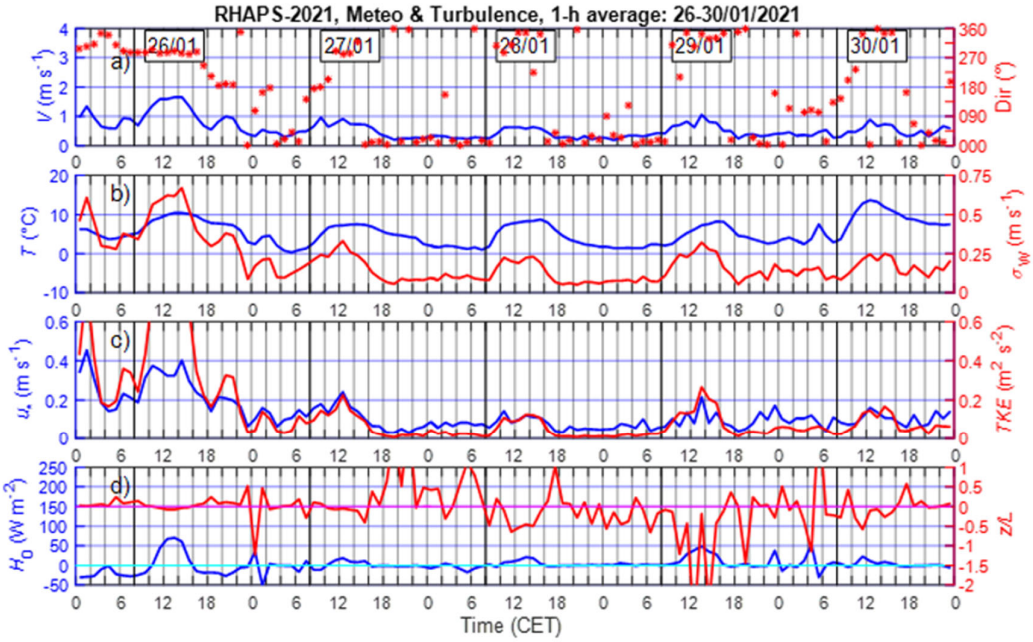

Figure S7. Time series of the wind speed (blue line) and direction (red line) (a), temperature (blue line) and variance of the vertical velocity (red line)(b) , friction velocity (blue line) and TKE(red line) (c), and heat flux (blue line) and Z/L (red line) (d) during the SIOP1 (26 to 30 January 2021).

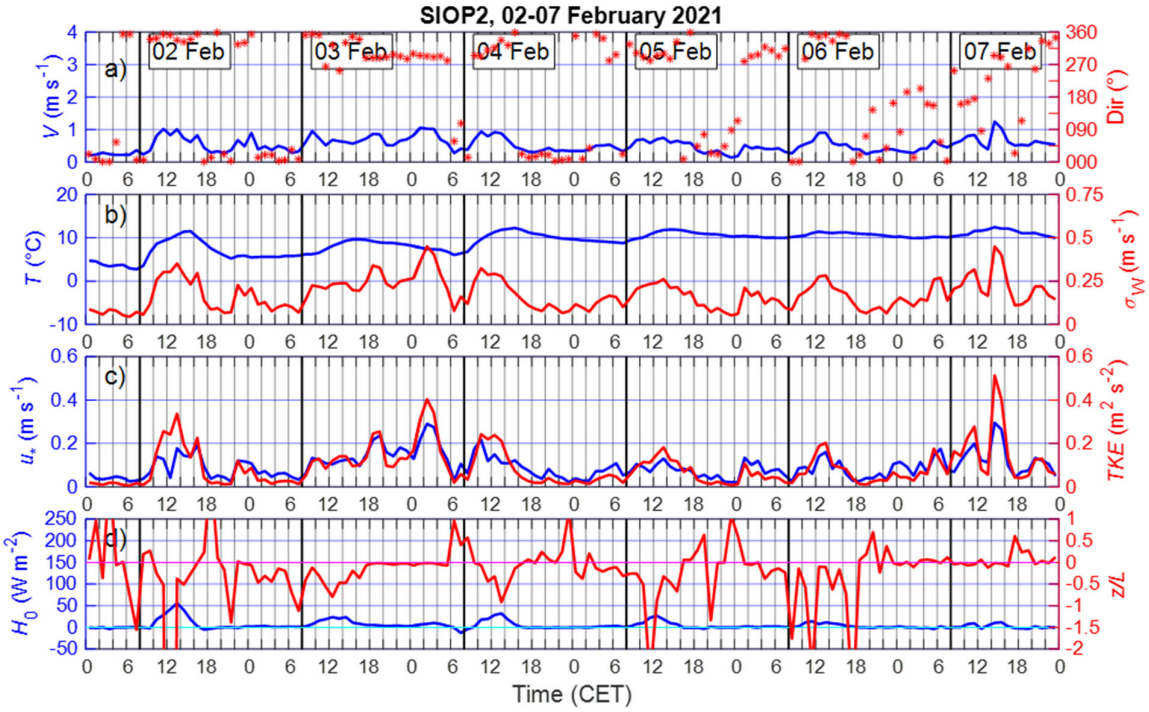

Figure S8. Time series of the wind speed (blue line) and direction (red line) (a), temperature (blue line) and variance of the vertical velocity (red line)(b) , friction velocity (blue line) and TKE(red line) (c), and heat flux (blue line) and Z/L (red line) (d) during the SIOP2 (2 to 7 February 2021).

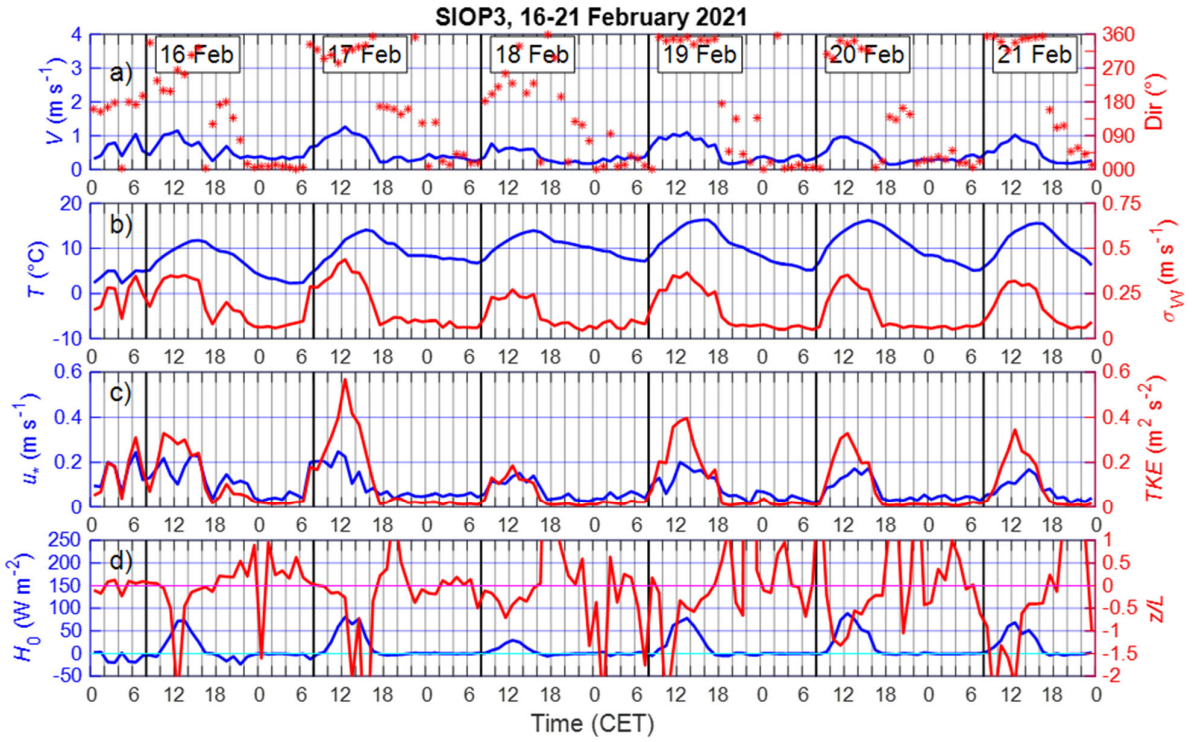

Figure S9. Time series of the wind speed (blue line) and direction (red line) (a), temperature (blue line) and variance of the vertical velocity (red line)(b) , friction velocity (blue line) and TKE(red line) (c), and heat flux (blue line) and Z/L (red line) (d) during the SIOP3 (16 to 21 February 2021).

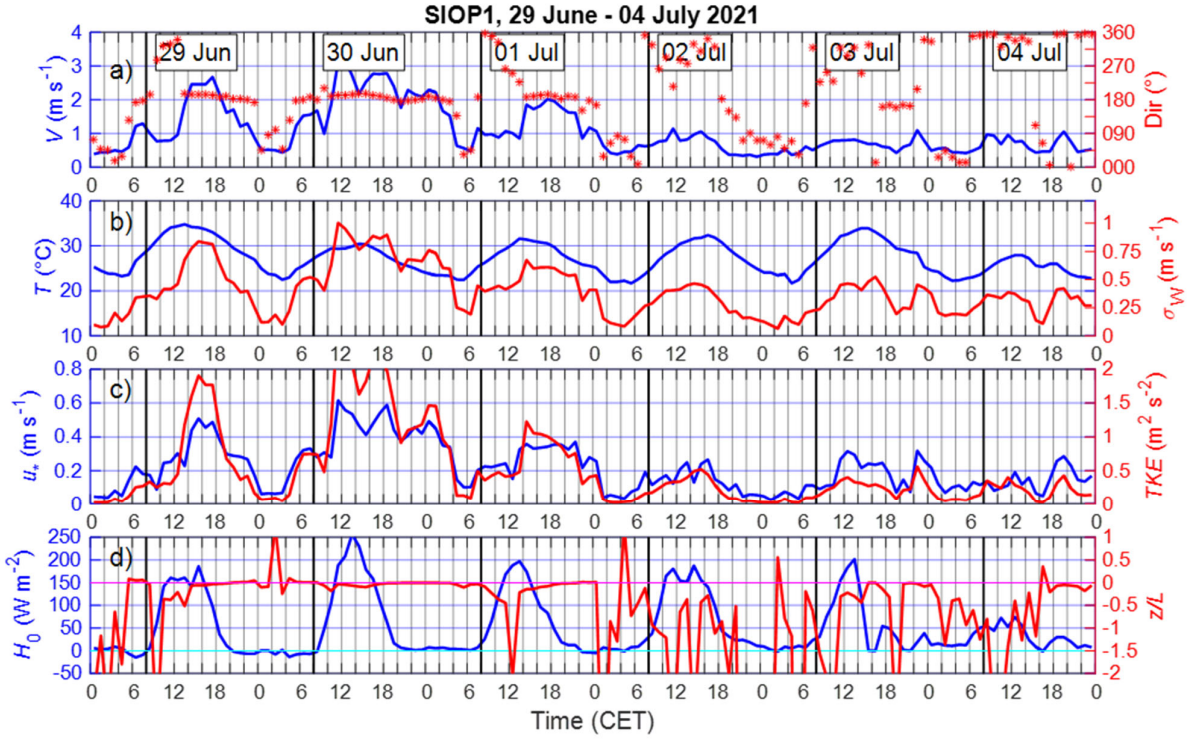

Figure S10. Time series of the wind speed (blue line) and direction (red line) (a), temperature (blue line) and variance of the vertical velocity (red line)(b) , friction velocity (blue line) and TKE(red line) (c), and heat flux (blue line) and Z/L (red line) (d) during the summer SIOP (29 June to 4 July 2021).

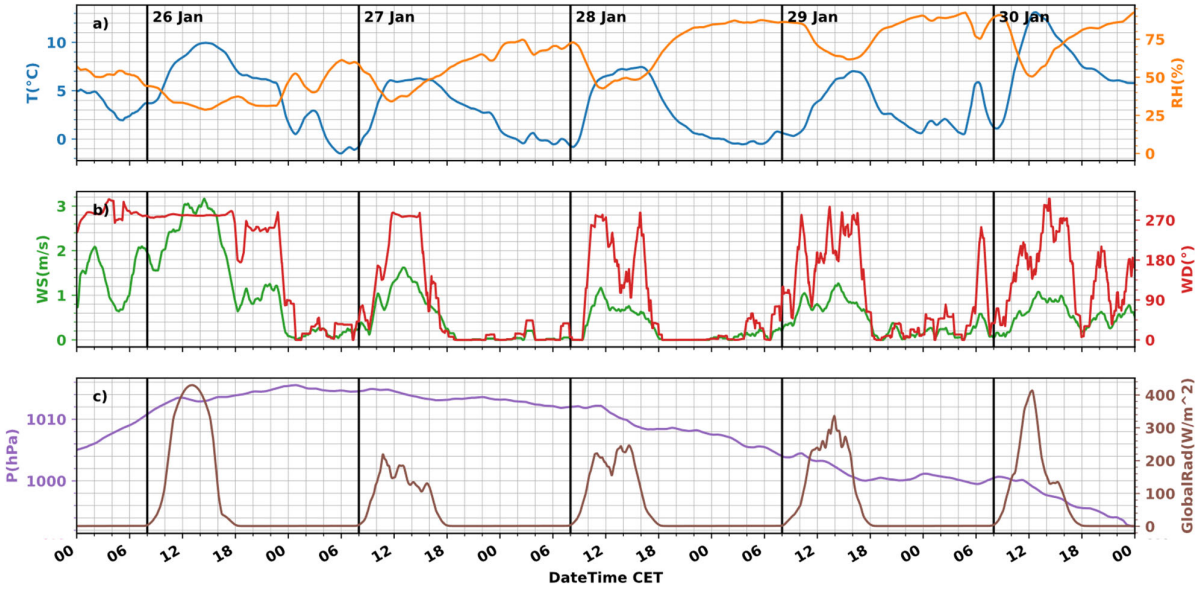

Figure S11. : Meteorological variables during SIOP1.

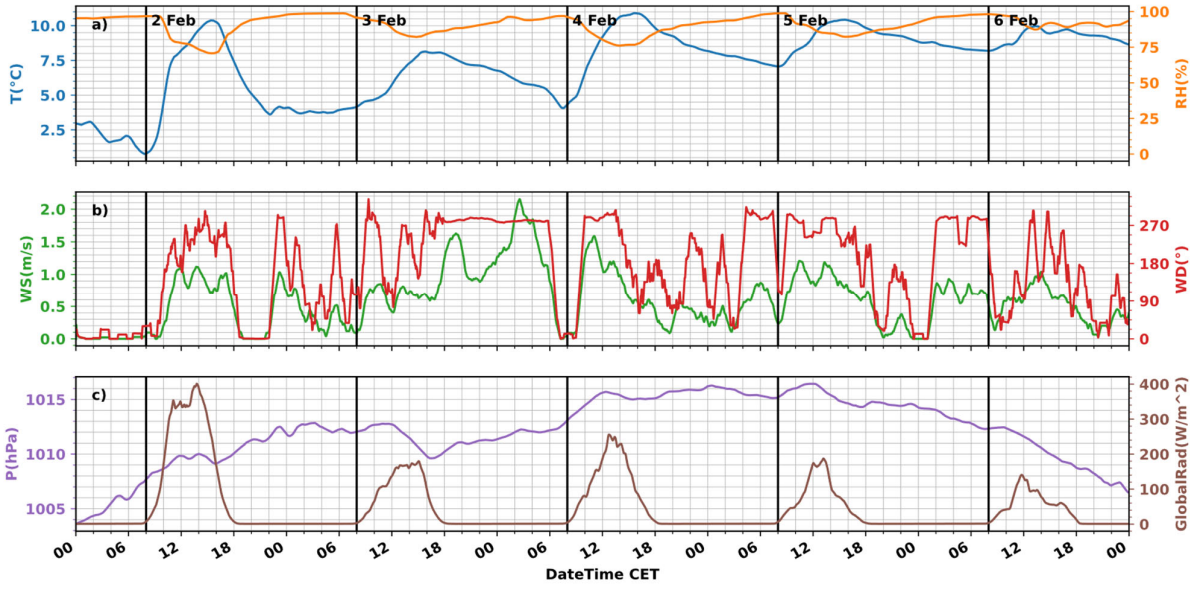

Figure S12. : Meteorological variables during SIOP2.

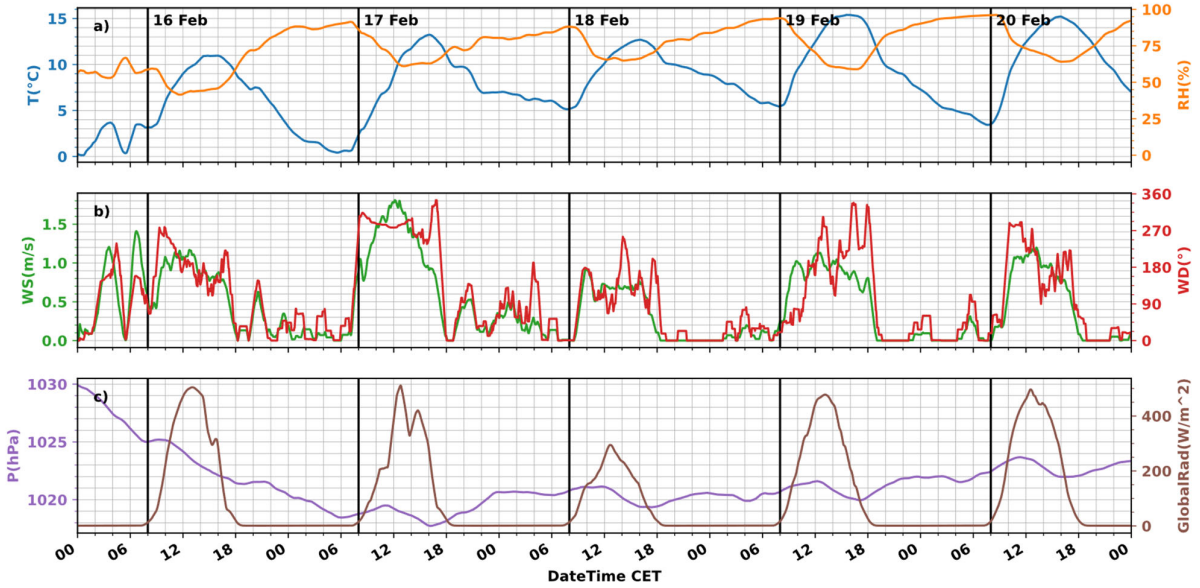

Figure S13. : Meteorological variables during SIOP3.

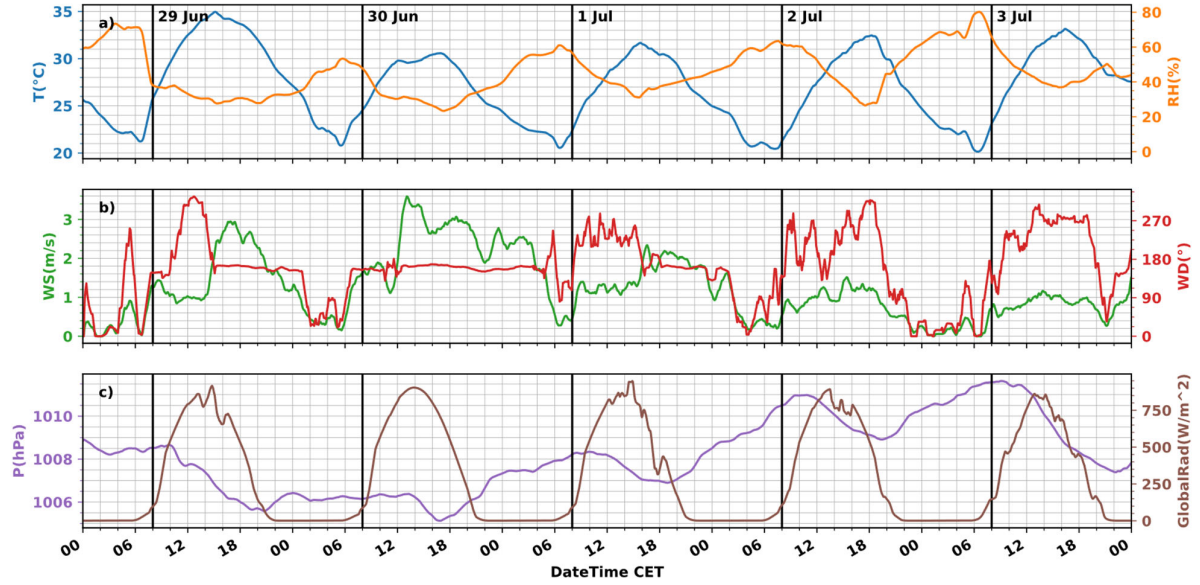

Figure S14. : Meteorological variables during SIOP4.

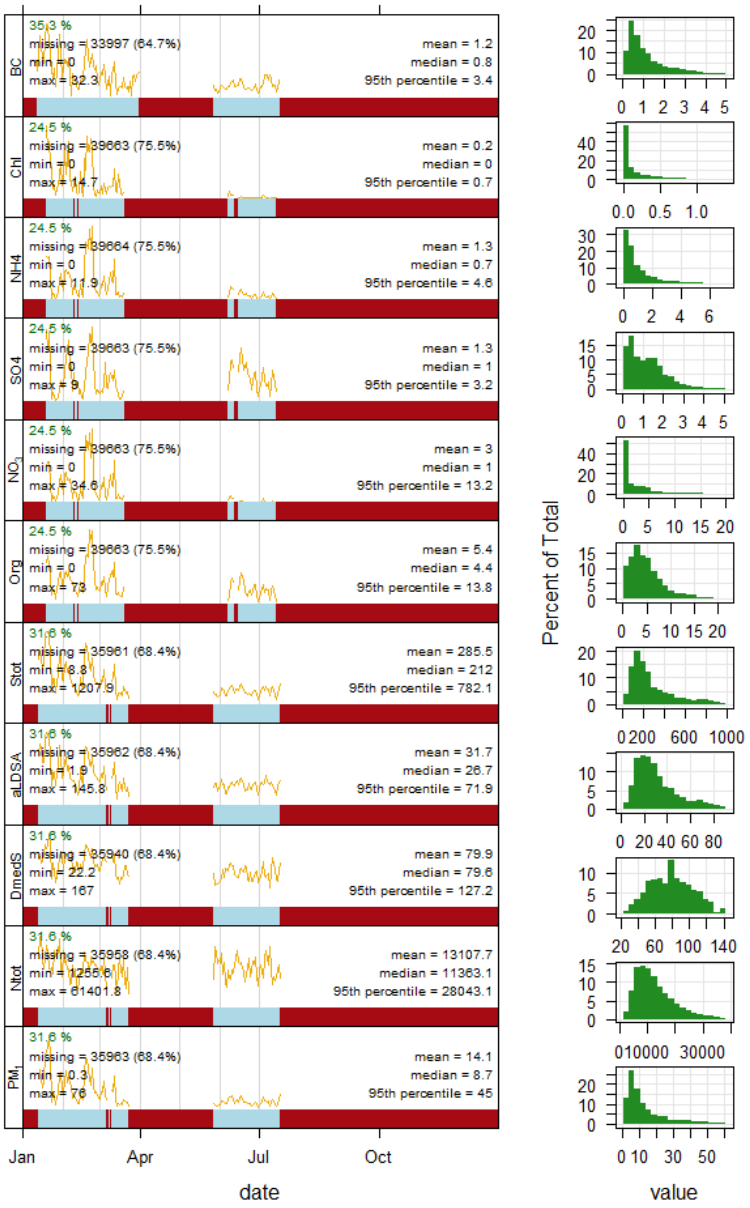

Figure S15. Time plots, statistics and data coverages of selected aerosol properties during the field campaigns. From top to bottom: Black Carbon, and non-refractory Choride, ammonium,sulfate, nitrate, organic aerosol mass concentration in PM1, total surface area concentration (Stot), alveolar Lung Deposited Surface Area (aLDSA), surface-weighted median particle diameter (Dmed), total number concentration (Ntot), and PM1 mass concentration (reconstructed by SMPS data) .

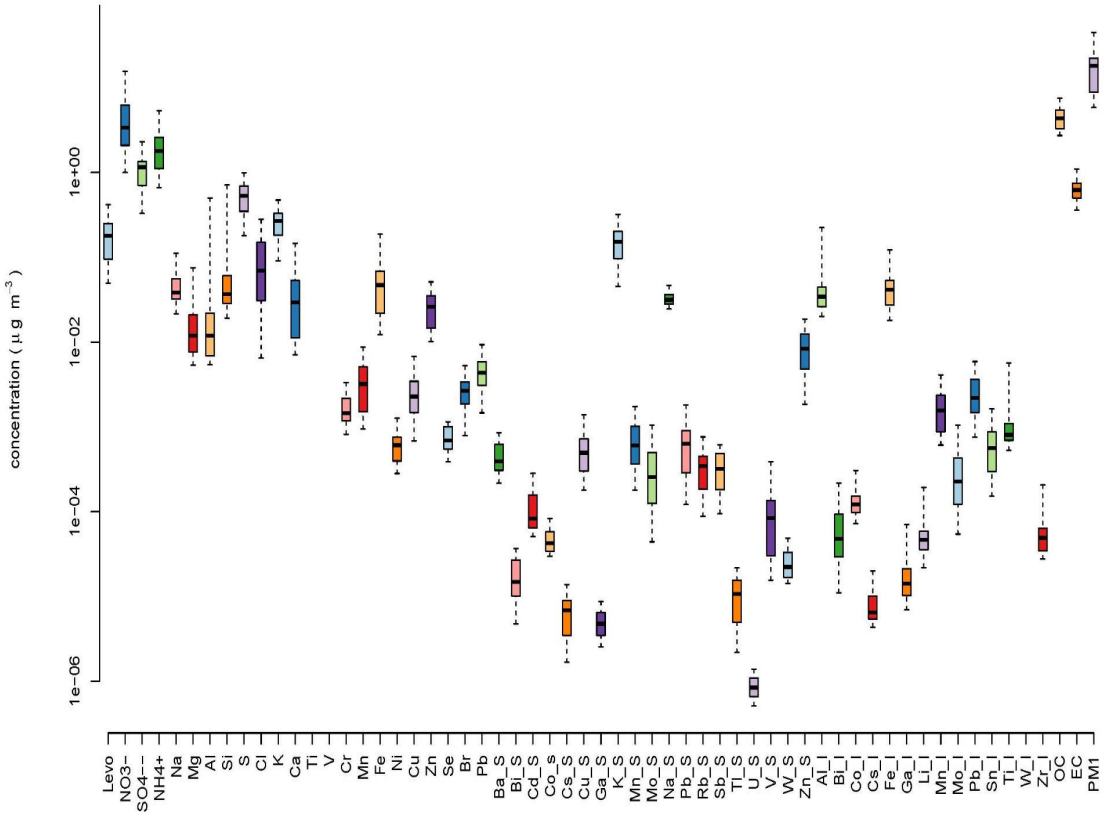

Figure S16. Overview of median (box plot), interquartile range (box plot), 9-95th percentiles (whisker plot) of PM_1 chemical components detected at the rural site of SPC during the winter campaign (I relates to insoluble, and S to soluble metal fractions).

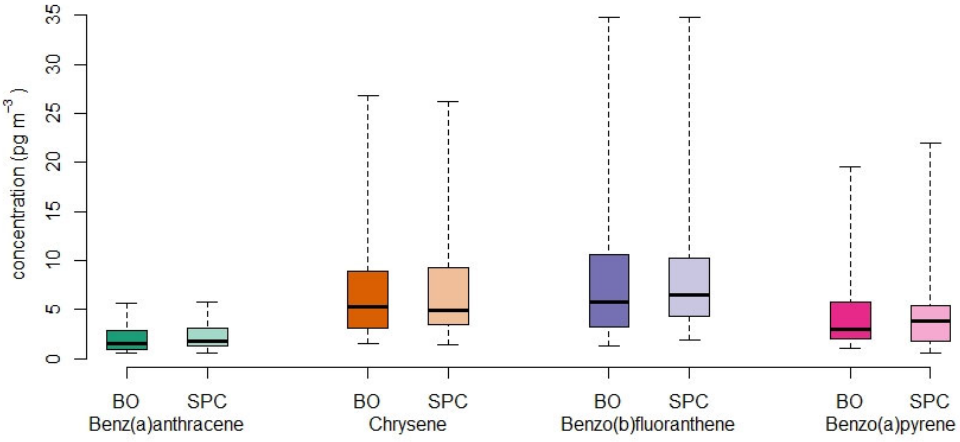

Figure S17. Overview of median (box plot), interquartile range (box plot), 9-95th percentiles (whisker plot) of PAHS detected in PM_1 samples at both sites during the winter campaign.

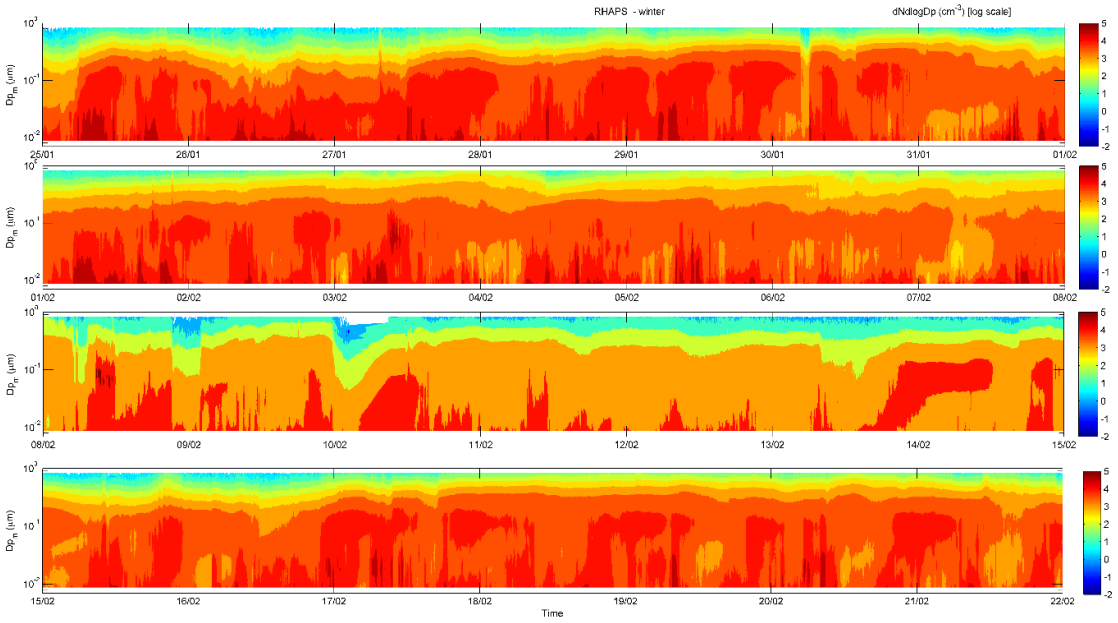

Figure S18. Full particle number size distribution measured in selected periods of the winter IOPs, including the four SIOPs.

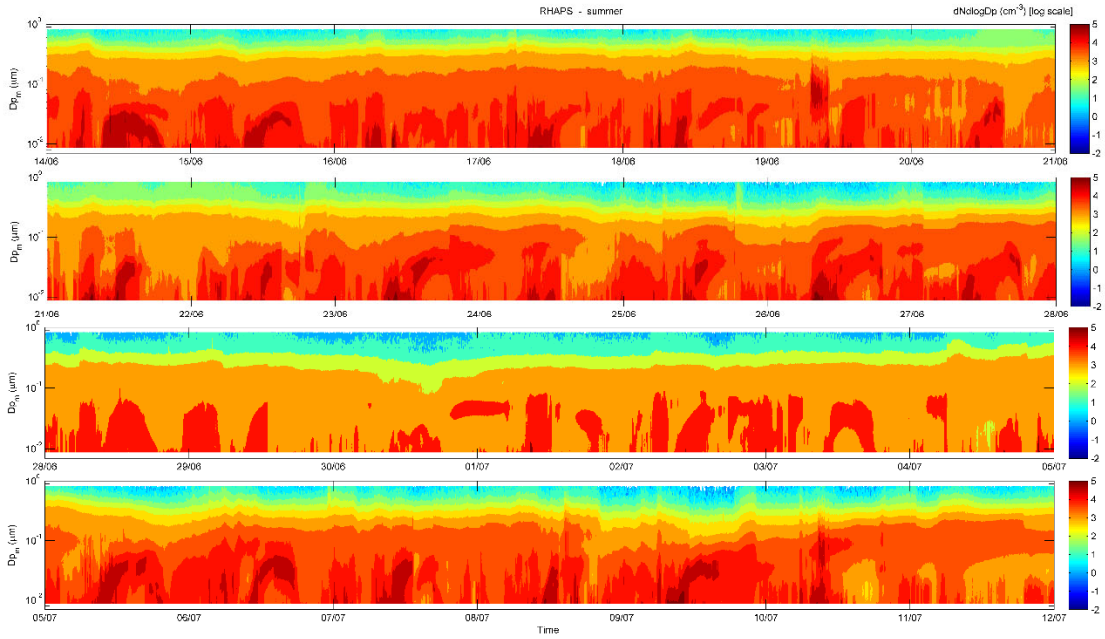

Figure S19. Full particle number size distribution measured in selected periods of the summer IOPs, including the four SIOPs.

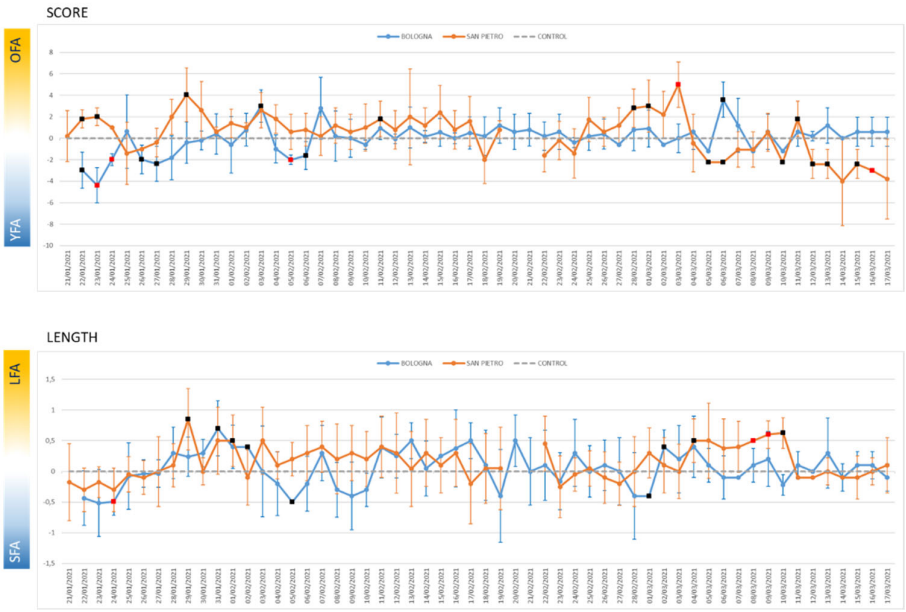

Figure S20. Development degree variations of the winter season reported as old-/young- for age (OFA/YFA) or large-/small- for age (LFA/SFA). Significance: black square $p<0.05$; red square $p<0.001$. Gray dotted line: control.

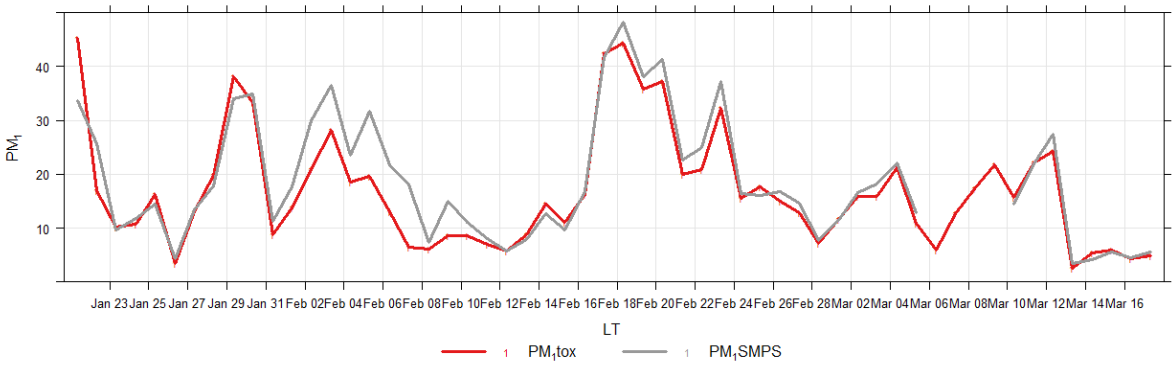

Figure S21. : Trends of PM1 mass concentration from the reference instruments and reconstructed from the SMPS.

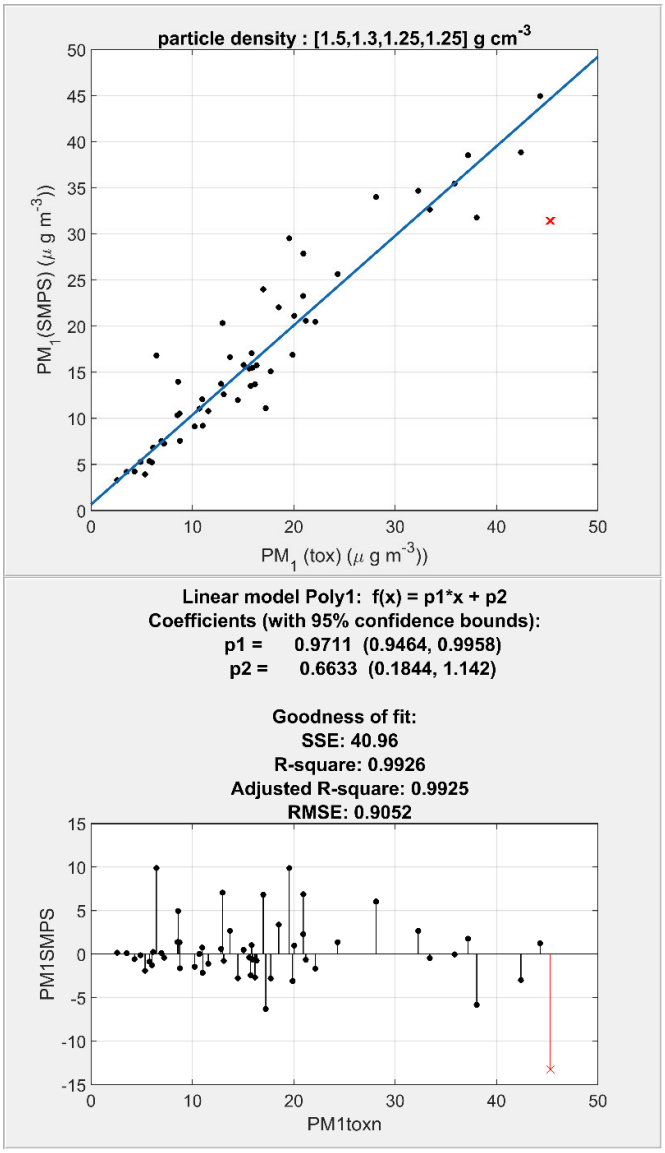

Figure S22. Goodness of the fit of the PM1 mass concentration from the reference instruments and reconstructed from the SMPS.

SUPPLEMENTARY TABLES

Table S1. MDL for species detected by Ion Cromatography.

Species	MDL
	ppm mL^{-1}
Cl^-	0.03
NO_3^-	0.05
SO_4^{2-}	0.05
Na^+	0.001
NH_4^+	0.03
K^+	0.03
Mg^{2+}	0.03
Ca^{2+}	0.002
Levoglucosan	0.01

Table S2. ChAMBRe instrumentation summary.

Instrument/Monitor	Measured quantity	Operative range
HMT334 Vaisala® Humicap® transmitter	Relative Humidity	0 – 90% RH
		90 – 100% RH
	Temperature	15 – 25°C
Pressure Gauges MKS 910 Dual-Trans™	Inner pressure	15 – 1000 mbar
		10^{-3} – 15 mbar
		5×10^{-4} – 2×10^{-3} mbar
Vaisala BAROCAP® PTB110	Outer pressure	5×10^{2} – 1.1×10^{3} mbar
Envea AC32e	NO_x(NO_2/NO)	0.2ppb – 10 ppm
Envea O342e	O_3	0.2ppb – 10 ppm
Envea AF22e	SO_2	0.4ppb – 10 ppm
Envea VOC72M	BTEX	0.02 – 310 ppb(Benzene)
Envea CO12e	CO/CO2	0.05 – 2000ppm
SMPS System TSI DMA model 3080 TSI W-CPC model 3789	Aerosol size distribution and concentration	10 -1000nm
Optical particle sizer TSI OPS model 3330	Aerosol size distribution and concentration	0.3 – 10 μm
UV-LIF bio—aerosol sensor DMT WIBS-NEO	Aerosol size distribution and concentration	2.5 – 30 μm
Photoacoustic Extinctiometers DMT PAXs (= 405, 532,870 nm)	Absorption extinction scattering coefficients	< 1 Mm^{-1} – 40000 Mm^{-1}

Table S3. : the m/z ratio and retention time of the analytes and IS.

Analyte	m/z ratio	RT
Benzo(α)anthracene -D12 (IS)	240	20,38
Benzo(α)anthracene	228	20,43

Crysene	228	20,52
Benzo(β)fluoranthene	252	22,84
Benzo(α)pyrene	252	23,50

Table S4. trace metals in PM1 samples collected in BO during winter and summer IOPs (in ng/m^3).

	BO_winter IOPs				BO_summer IOPs			
	# samples	median	5°perc	95°perc	# samples	median	5°perc	95°perc
Ba _s	35	0.492	0.250	0.917	36	1.87	0.779	3.46
Bi _s	52	0.023	0.006	0.088	27	0.009	0.005	0.026
Cd _s	43	0.090	0.045	0.183	0			
Co_s	0				24	0.049	0.027	0.134
Cs _s	53	0.009	0.002	0.018	24	0.002	0.001	0.004
Cu _s	56	0.646	0.161	2.05	35	0.540	0.120	1.10
Ga_s	41	0.006	0.002	0.011	19	0.003	0.002	0.007
K_s	54	136.7	28.3	306.7	26	39.1	25.1	95.9
Mn_s	55	0.647	0.156	2.82	33	0.437	0.220	1.00
Mo_s	54	0.348	0.060	1.45	36	0.184	0.080	0.497
Na_s	42	31.1	24.0	66.6	0			
Pb_s	52	0.765	0.177	2.36	23	0.217	0.099	0.760
Rb_s	56	0.318	0.055	0.740	0			
Sb_s	50	0.370	0.106	0.849	30	0.226	0.104	0.490
Tl_s	55	0.012	0.002	0.025	31	0.004	0.002	0.008
U_s	34	0.001	0.001	0.002	21	0.001	0.001	0.002
V_s	49	0.083	0.025	0.479	36	0.175	0.039	0.548
W_s	34	0.027	0.015	0.066	0			
Zn_s	56	8.52	1.89	25	35	3.24	0.919	7.90
Al_i	56	37.6	21.8	121.3	34	34.5	22.9	228.1
Bi_i	56	0.047	0.018	0.145	36	0.030	0.015	0.071
Co_i	55	0.120	0.072	0.288	36	0.113	0.069	0.338
Cs_i	50	0.006	0.004	0.016	34	0.006	0.004	0.021
Fe_i	55	50.7	25.9	143.5	36	54.3	31.1	165.1
Ga_i	54	0.013	0.008	0.035	36	0.010	0.006	0.061
Li_i	56	0.046	0.023	0.117	36	0.033	0.019	0.156
Mn_i	56	1.58	0.732	3.88	36	1.16	0.83	2.54
Mo_i	56	0.263	0.059	0.834	36	0.116	0.052	0.276
Pb_i	56	1.96	0.869	4.93	35	0.559	0.389	1.34
Sn_i	56	0.487	0.156	1.55	36	0.326	0.196	0.658
Ti_i	56	0.943	0.544	3.36	35	0.870	0.529	4.40
W_i	41	0.033	0.022	0.086	0			
Zr_i	56	0.074	0.037	0.131	36	0.084	0.045	0.158

Table S5. major PM1 components detected in BO during winter and summer IOPs (in ng/m3).

	BO_winter IOPs				BO_summer IOPs			
	# samples	median	5°perc	95°perc	# samples	median	5°perc	95°perc
PM1	56	15985	4270	43955	36	7999	4319	12899
OC	56	3574	2052	5966	36	2345	1536	3404

EC	56	774	399	1310	36	343	226	451
NO_3^-	56	2930	772	13530	36	244	157	941
SO_4^{--}	56	811	190	1834	36	1258	507	2240
NH_4^+	53	1232	359	4945	36	537	211	1048
Levoglucosan	56	179	49	365	21	24	9.3	36.6
Na	56	28	13	68	32	28	7.1	77
Mg	30	13	5.6	56	32	16	4.7	93
Al	50	13	4.7	221	35	40	15	389
Si	56	48	20	490	35	135	62	891
Cl	54	44	8.3	286	35	8.5	5.0	16
K	56	211	86	408	35	47	24	150
Ca	54	52	11	177	35	89	29	264
Ti	0				32	1.8	0.8	18
V	0				18	0.8	0. 7	2.6
Cr	45	1.3	0.7	2.9	25	0.7	0.5	1.2
Mn	54	2.7	0.8	7.7	35	1.6	1.1	4.2
Fe	56	57	15	136	35	53	26	209
Ni	51	0.5	0.3	1.1	32	0.4	0.2	0.8
Cu	56	2.7	1.0	5.2	35	1.7	0.9	2.7
Zn	56	21	11	42	35	5.6	3.0	10
Se	38	0.6	0.4	1.2	32	0.4	0.2	0.9
Br	56	2.9	1.3	6.9	35	1.8	0.7	3.1
Pb	55	3.8	1.4	11	34	1.5	0.6	3.0